www.czasopisma.pan.pl PAN POLSKA AKADEMIA NAUK www.journals.pan.pl

BULLETIN OF THE POLISH ACADEMY OF SCIENCES
TECHNICAL SCIENCES
Vol. 54, No. 4, 2006

Axi-symmetric ice sheet flow with evolving anisotropic fabric

R. STAROSZCZYK*

Institute of Hydro-Engineering, Polish Academy of Sciences, 17 Waryńskiego St., 71-310 Szczecin, Poland

Abstract. An axially symmetric, gravity driven, steady flow of a grounded polar ice sheet with a prescribed temperature field is considered. The ice is treated as an incompressible, non-linearly viscous, anisotropic fluid, the internal structure (fabric) of which evolves as ice descends from the free surface to depth in an ice sheet. The evolution of the ice fabric is described by an orthotropic constitutive law which relates the deviatoric stress to the strain-rate, strain, and three structure tensors based on the current (rotating) principal stretch axes. The solution of the problem is constructed as a leading-order approximation derived from asymptotic expansions in a small parameter that reflects the small ratio of stress and velocity gradients in the lateral direction of the ice sheet to those in the thickness direction. Numerical simulations of the flow problem have been carried out for various sets of rheological parameters defining the limit strength of the anisotropic fabric in ice. The results of calculations illustrate the influence of the ice anisotropy, basal melt conditions and temperature field in ice on the glacier thickness and lateral span, and on the depth profiles of the flow velocity.

Key words: polar ice, viscosity, evolving anisotropy, orthotropy, constitutive law.

1. Introduction

Ice cores retrieved from large polar ice caps in Antarctica and Greenland show strong anisotropic fabrics, in which individual ice crystal c-axes (axes of crystal hexagonal symmetry) are aligned along some preferential directions [1]. These fabrics develop, and subsequently evolve, in the material in response to changing stress and deformation states which ice experiences during its descent from the free surface to depth in an ice sheet. As a result, the microscopic structure of the material varies with ice depth, and this translates into considerable changes in the macroscopic properties of the medium. For instance, macroscopic shear viscosity of ice that is found near a glacier base is, typically, by up to one order of magnitude smaller than the viscosity of initially isotropic ice that is deposited on the free surface. Smaller, but also significant, difference between the surface and the basal ice occurs in terms of its axial viscosity. Such dramatic changes in the viscous properties of the medium with increasing depth must have important consequences for the overall flow of polar ice masses (which, on geophysical scales, deform mainly by viscous creep); therefore, the mechanism of evolving anisotropy should be incorporated into realistic models describing the behaviour of ice. However, in current large-scale numerical models used to simulate the past and future climatic scenarios and their effects on the flow of ice caps, the evolving anisotropy of ice is commonly ignored and, for simplicity, the material is treated as isotropic. In such models, in order to account for the variation of creep properties of ice to reflect its anisotropy, the material rheology is described in terms of so-called enhancement factors [2], the values of which are chosen ad hoc to fit available empirical data (measurements of the free surface velocities and ice core fabrics). Only few attempts have been made to extend this approach by employing a method in which a single, general relation between the flow field and the observed fabric is used throughout a whole ice sheet. An example are the papers by Mangeney et al [3,4], who adopted the transversely isotropic fabric corresponding to that drilled in Central Greenland to solve numerically a steady-state flow problem of the ice sheet under isothermal conditions. In these papers, however, the empirically derived fabric is a function of the ice depth only, since no constitutive equation that relates the fabric evolution to the flow field is included in the analysis. Hence, the fabric adopted in the latter papers is *static*, that is, uncoupled from the flow field.

In this work we make a step further, and solve a more difficult problem, in which the flow field is not only a function of the anisotropic fabric, but also the fabric itself is a function of the flow field variables which determine how the fabric evolves to adjust to varying local flow conditions. Accordingly, there is full coupling between the flow and the *evolving* fabric, so that the fabric determination constitutes an integral part of the problem solution. To this aim, we describe the ice fabric evolution by applying a constitutive law formulated by Staroszczyk and Morland [5], in which the medium is treated as an anisotropic viscous fluid with orthotropic material symmetries, and which expresses the deviatoric stress in terms of the strain-rate and the current strain. The law involves two ice response coefficient functions which have been determined by correlation with the observed viscous behaviour of ice at indefinitely large deformations. Furthermore, the adopted law incorporates strong non-linear effects of temperature and the deviatoric stress magnitudes on the viscous behaviour of ice.

We analyse a steady flow of a radially symmetric ice sheet which slides on a rigid bedrock, and whose motion is driven by gravity forces. At the free surface of the sheet a snow accumulation rate distribution is assumed, defining the mass fluxes into and out of the glacier across its top surface. Similarly, an ice

*e-mail: rstar@ibwpan.gda.pl

melt rate is assumed at the base of the sheet to define the mass flux across the bottom surface. The temperature field within the ice sheet is also prescribed, so that the mass and momentum balance equations are uncoupled from the energy balance equations. For the above input conditions, the unknown geometry of the glacier, that is, the free surface profile (including the maximum glacier thickness and the lateral span) is determined. The main purpose of the analysis is to investigate how the anisotropy of ice influences the overall flow of the ice sheet, and, in particular, how it affects the ice velocity field (which is important to know when choosing locations for polar stations or ice core drilling sites).

The solution of the problem is constructed by a method of asymptotic expansions. Hence, we take advantage of a small parameter ϵ reflecting the small ratio of stress and velocity gradients in the lateral direction to those in the ice thickness direction, and use this parameter to scale the ice flow equations and the boundary conditions. Then, all terms of order ϵ and smaller compared to unity are neglected in the ensuing equations with the aim to reduce them to simpler, leading-order, forms. The reduced equations are subsequently integrated through the ice thickness to eliminate one spatial coordinate. This gives rise to a two-point boundary-value problem for a second order parabolic differential equation, which is solved numerically to calculate the free surface profile. Simultaneously, a set of differential equations of a hyperbolic type is also integrated along the ice particle paths (characteristics) to determine the evolution of the material properties as ice moves inside the glacier. The results of calculations, carried out for different sets of ice rheological parameters, different basal melt rates and different temperature distributions, illustrate the effects of the latter factors on the glacier geometry (thickness and span), and the depth profiles of the ice velocities.

2. Flow problem formulation

The problem is solved in cylindrical polar coordinates (r, θ, z), with the r axis on the horizontal plane, and the vertical axis z directed upwards. It is assumed that the ice sheet geometry and all variables involved are symmetric about the z axis, so that they are independent of the polar angle θ and, hence, they are functions of only r and z. The ice sheet cross-section, with the adopted coordinates and other relevant notations, is sketched in Fig. 1. The ice sheet geometry is defined by the free surface elevation $z = h(r)$ and the bed elevation $z = f(r)$. The ice sheet ends at the margin, where the ice thickness becomes zero, $h = f$. The free surface is traction free, with the stress in ice measured relative to atmospheric pressure assumed to be uniform. At the free surface there is an ice accumulation, a mass flux per unit area, q, as ice enters the glacier due to precipitation or ablation/melting, respectively. The accumulation rate q, in general a function of h and r, is regarded positive (snowfall) at higher altitudes in central regions of the sheet, and negative (ablation/melting) at lower altitudes near the margins. At the bed, there is also a mass flux, denoted by b, due to ice melting ($b > 0$) or refreezing ($b < 0$). Moreover, depending on local conditions, basal sliding may, or may not, occur at the bed. There can also be heat fluxes across the glacier boundaries, but these are neglected in this analysis.

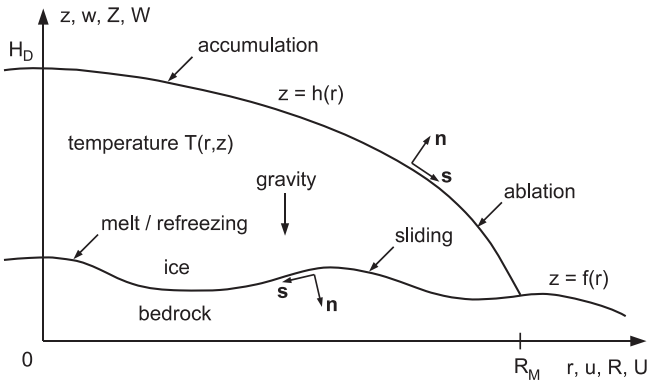

Fig. 1. Ice sheet geometry

The velocity field $\boldsymbol{v}$ in our steady flow is described by the radial and vertical components $u(r, z)$ and $w(r, z)$, respectively. The rate of deformation of ice, the viscous fluid, is measured by the strain-rate tensor $\boldsymbol{D}$, the non-vanishing components of which are expressed in terms of the velocities by

$$D_{rr} = \frac{\partial u}{\partial r}, \quad D_{\theta\theta} = \frac{u}{r}, \qquad D_{zz} = \frac{\partial w}{\partial z}, \quad D_{rz} = \frac{1}{2}\left(\frac{\partial u}{\partial z} + \frac{\partial w}{\partial r}\right). \tag{1}$$

It is commonly assumed in glaciology that the viscous deformation (creep) of ice does not depend on the mean pressure, p, so that the medium can be treated as an incompressible material, the behaviour of which is governed by the stress deviator, $\boldsymbol{S}$. Hence, the mass balance equation becomes the ice incompressibility condition $\mathrm{tr}\,\boldsymbol{D} = 0$ (tr is the trace operator), which in components reads

$$\frac{\partial u}{\partial r} + \frac{u}{r} + \frac{\partial w}{\partial z} = 0. \tag{2}$$

The deviatoric stress is defined in terms of the Cauchy stress $\boldsymbol{\sigma}$ and the pressure by the decomposition

$$\boldsymbol{S} = \boldsymbol{\sigma} + p\boldsymbol{I}, \quad p = -\tfrac{1}{3}\,\mathrm{tr}\,\boldsymbol{\sigma}, \tag{3}$$

where $\boldsymbol{I}$ is the unit tensor. Relations (3) give the non-zero deviatoric stress components

$$S_{rr} = \sigma_{rr} + p, \quad S_{\theta\theta} = \sigma_{\theta\theta} + p, \qquad S_{zz} = \sigma_{zz} + p, \quad S_{rz} = \sigma_{rz}. \tag{4}$$

The horizontal radial and vertical momentum balances, in the absence of inertia forces in our extremely slow flow, become the equilibrium relations under gravity

$$\frac{\partial S_{rr}}{\partial r} + \frac{S_{rr} - S_{\theta\theta}}{r} + \frac{\partial S_{rz}}{\partial z} - \frac{\partial p}{\partial r} = 0, \tag{5}$$

$$\frac{\partial S_{rz}}{\partial r} + \frac{S_{rz}}{r} + \frac{\partial S_{zz}}{\partial z} - \frac{\partial p}{\partial z} - \varrho g = 0, \tag{6}$$

and the circumferential balance is automatically satisfied because of the radial symmetry of the problem. In the latter equations, ϱ denotes the ice density, and g is the gravitational acceleration.

The mass and momentum balances (2), (5) and (6) are subject to boundary conditions at the free surface and the bed, expressing the interactions of the glacier with the atmosphere and the bedrock. Define the unit outward normal and tangent vectors $\boldsymbol{n}$ and $\boldsymbol{s}$ in a right-hand sense, as depicted in Fig. 1. Then, the zero traction condition at $z = h(r)$ is expressed in terms of vanishing normal and tangential components $t_n = \boldsymbol{n} \cdot \boldsymbol{\sigma n}$ and $t_s = \boldsymbol{s} \cdot \boldsymbol{\sigma n}$ in the Orz plane. Accordingly,

$$z = h(r):$$
$$\Delta_h^2 t_n = -\Delta_h^2 p + [h'(r)]^2 S_{rr} + S_{zz} - 2h'(r) S_{rz} = 0, \quad (7)$$
$$z = h(r):$$
$$\Delta_h^2 t_s = h'(r)(S_{zz} - S_{rr}) + \{1 - [h'(r)]^2\} S_{rz} = 0, \quad (8)$$

where $(\cdot)'$ denotes differentiation with respect to the argument, and

$$\Delta_h = \{1 + [h'(r)]^2\}^{1/2}. \quad (9)$$

The prescription of mass flux across the free surface yields the kinematic condition in the form

$$z = h(r): \quad h'(r)u - w = \Delta_h q. \quad (10)$$

At the prescribed bed $z = f(r)$, normal and tangential tractions, t_n and t_s respectively, are expressed by

$$z = f(r):$$
$$\Delta_f^2 t_n = -\Delta_f^2 p + [f'(r)]^2 S_{rr} + S_{zz} - 2f'(r) S_{rz}, \quad (11)$$
$$z = f(r):$$
$$\Delta_f^2 t_s = f'(r)(S_{zz} - S_{rr}) + \{1 - [f'(r)]^2\} S_{rz}, \quad (12)$$

where

$$\Delta_f = \{1 + [f'(r)]^2\}^{1/2}, \quad (13)$$

and normal and tangential velocities at the bed, v_n and v_s respectively, are given by

$$z = f(r): \quad \Delta_f v_n = f'(r)u - w, \quad \Delta_f v_s = -u - f'(r)w. \quad (14)$$

The kinematic condition prescribing the normal basal mass flux due to ice melt (drainage) or refreezing becomes

$$z = f(r): \quad f'(r)u - w = \Delta_f b. \quad (15)$$

At the bed either no-slip or sliding can occur. In the former case, the ice particle velocity component tangential to the surface $f(r)$ is zero, that is, $v_s = 0$. This, in view of $(14)_2$, is equivalent to

$$u + f'(r)w = 0. \quad (16)$$

In the case of sliding, the basal tangential traction t_s is related to the tangential velocity v_s and the normal pressure $p = -t_n$ by a sliding law. We adopt a linear form of the latter, defined by

$$z = f(r): \quad t_s = \lambda t_n v_s, \quad (17)$$

where λ is a constant friction coefficient. The proportionality of t_s to t_n ensures that, as a margin is approached and the pressure approaches zero, the free surface slope at a margin is bounded (Morland and Johnson [6]); in the case of no-slip basal conditions, the slope at the margin is unbounded.

3. Orthotropic constitutive law

The solution of the momentum balance equations, (5) and (6), requires a constitutive law for the deviatoric stress — the mean pressure p is not prescribed by the constitutive relation due to the ice incompressibility. Various aspects of the constitutive modelling of anisotropic ice are discussed in detail by Staroszczyk [7], below we briefly present only those elements which are relevant in the context of this work.

We adopt here the law in the orthotropic form proposed in [5], which is a modification of an earlier constitutive model formulated by Staroszczyk and Morland [8]; an alternative theory is presented by Morland and Staroszczyk in [9]. The adopted law is expressed in an additive form, in which the viscous response of the material is decomposed into isotropic and anisotropic parts, with the latter describing the evolution of the oriented fabric from its initial isotropic state. The isotropic part relates the deviatoric stress to the strain-rate only, alike the conventional isotropic viscous fluid flow law. The anisotropic part, apart from the strain-rate, also includes the dependence on the strain, introduced to allow the evolution of the oriented structure of the medium to be followed while the ice undergoes changing stress/strain regimes during its motion. Hence, we apply the law

$$\boldsymbol{S} = \mu_0 \Big\{ 2\boldsymbol{D} + \sum_{s=1}^{3} \tilde{f}(b_s) \big[\boldsymbol{M}^{(s)} \boldsymbol{D} + \boldsymbol{D} \boldsymbol{M}^{(s)} - \tfrac{2}{3} \operatorname{tr}(\boldsymbol{M}^{(s)} \boldsymbol{D}) \boldsymbol{I} \big] + \tilde{g}(K) \big[\boldsymbol{B}\boldsymbol{D} + \boldsymbol{D}\boldsymbol{B} - \tfrac{2}{3} \operatorname{tr}(\boldsymbol{B}\boldsymbol{D}) \boldsymbol{I} \big] \Big\}, \quad (18)$$

where μ_0 is the viscosity of isotropic ice, $\tilde{f}(b_s)$ $(s = 1, 2, 3)$ and $\tilde{g}(K)$ denote fabric response coefficients, $\boldsymbol{B}$ is the left Cauchy-Green deformation tensor, and b_s and $K = \operatorname{tr} \boldsymbol{B}$ are the invariants of $\boldsymbol{B}$. $\boldsymbol{M}^{(s)}$ $(s = 1, 2, 3)$ are three structure tensors which describe the orientation in space of the privileged directions in the material. The latter are aligned along the current directions of the principal stretch axes, and define the three (rotating) planes of the orthotropic symmetry of the medium. Thus, they are defined by the outer products of the normalized eigenvectors of $\boldsymbol{B}$, that is,

$$\boldsymbol{M}^{(s)} = \boldsymbol{e}^{(s)} \otimes \boldsymbol{e}^{(s)}, \quad \boldsymbol{B}\boldsymbol{e}^{(s)} = b_s \boldsymbol{e}^{(s)}, \quad |\boldsymbol{e}^{(s)}| = 1 \quad (s = 1, 2, 3), \quad (19)$$

where b_s, the invariant arguments of the functions $\tilde{f}$ and $\tilde{g}$, are the eigenvalues of $\boldsymbol{B}$, and $\boldsymbol{e}^{(s)}$ are the eigenvectors of the latter. The specific forms of the fabric response functions have been constructed by first deducing some of their general properties, and then by correlating them with empirical results describing the viscous behaviour of ice [8]. The form of $\tilde{f}$ adopted in this work is defined by

$$\tilde{f}(b_s) = \tilde{f}_\infty - (\tilde{f}_\infty - \tilde{f}_0) \exp(-\zeta b_s^n), \quad \zeta > 0, \quad n > 0, \quad (20)$$

where n is a free parameter, and ζ is determined by the condition $\tilde{f}(1) = \tilde{f}'(1)$ [5]. The fabric response function $\tilde{g}$ is related

to $\tilde{f}$ by

$$\tilde{g}(K) = -\frac{\tilde{f}(b) - \tilde{f}(b^{-1})}{b - b^{-1}}, \quad 2b = K - 1 + \sqrt{(K-1)^2 - 4}\,. \tag{21}$$

The constants $\tilde{f}_0$ and $\tilde{f}_\infty$, appearing in (20), are given by

$$\tilde{f}_0 = E_s^{-1} - 1, \quad \tilde{f}_\infty = 6E_a^{-1} - 5E_s^{-1} - 1, \tag{22}$$

where E_a and E_s denote so-called enhancement factors for compression and shear, respectively. These two factors are measured in laboratory tests and their values denote the ratios of the isotropic ice viscosity to the anisotropic ice viscosity at indefinitely large, axial or shear, strains.

The isotropic ice viscosity μ_0 depends on temperature and the stress/strain-rate magnitude. This, strongly non-linear, dependence is expressed here in the form obtained by correlation with experimental results

$$\mu_0(T, J) = \frac{\sigma_0}{2D_0}\, a^{-1}(T)\, \psi^{-1}(J), \tag{23}$$

where T denotes absolute temperature, J is the second principal deviatoric stress invariant, and $\sigma_0 = 10^5$ Pa and $D_0 = 1\ \text{yr}^{-1} = 3.17 \times 10^{-8}\ \text{s}^{-1}$ (where 'yr' stands for the year) are normalizing stress and strain-rate magnitudes. The dimensionless functions a and ψ have the representations derived in [10]:

$$a(\bar{T}) = 0.68 \exp(12\bar{T}) + 0.32 \exp(3\bar{T}), \qquad \bar{T} = (T - 273.15\ \text{K})/\,[20\ \text{K}], \tag{24}$$

$$\psi(J) = 0.3336 + 0.32J + 0.0296J^2, \qquad J = \tfrac{1}{2}\,\text{tr}(\boldsymbol{S}/\sigma_0)^2. \tag{25}$$

The ice fabric is described in (18) by the left Cauchy-Green tensor $\boldsymbol{B}$, and this requires the deformation gradient tensor $\boldsymbol{F}$, since $\boldsymbol{B} = \boldsymbol{F}\boldsymbol{F}^T$ (the superscript T denotes the transpose). In our axially symmetric flow, $\boldsymbol{F}$ has five non-trivial components

$$F_{rr} = \frac{\partial r}{\partial r^*}, \quad F_{\theta\theta} = \frac{r}{r^*}, \quad F_{zz} = \frac{\partial z}{\partial z^*}, \quad F_{rz} = \frac{\partial r}{\partial z^*}, \quad F_{zr} = \frac{\partial z}{\partial r^*}, \tag{26}$$

where r^* and z^* denote the particle reference (material) coordinates. The evolution of the deformation field with time t is governed by the kinematic relation

$$\dot{\boldsymbol{F}} = \boldsymbol{L}\boldsymbol{F}, \quad \dot{F}_{ij} = \frac{\partial F_{ij}}{\partial t} + v_k \frac{\partial F_{ij}}{\partial x_k} \quad (i, j, k = r, \theta, z), \tag{27}$$

where the superimposed dot denotes material time derivative, and $\boldsymbol{L}$ is the velocity gradient tensor. The latter has five non-zero components given by

$$L_{rr} = \frac{\partial u}{\partial r}, \quad L_{\theta\theta} = \frac{u}{r}, \quad L_{zz} = \frac{\partial w}{\partial z}, \quad L_{rz} = \frac{\partial u}{\partial z}, \quad L_{zr} = \frac{\partial w}{\partial r}. \tag{28}$$

The relation (27) is equivalent to five first-order differential equations, though only four of them are independent due to the ice incompressibility constraint $\det \boldsymbol{F}$=1, that is,

$$F_{\theta\theta}(F_{rr}F_{zz} - F_{rz}F_{zr}) = 1. \tag{29}$$

4. Scaled equations

The solution of the complete set of equations governing the ice sheet flow, as given in Section 2, encounters serious numerical difficulties, and in fact is still beyond the reach of theoretical glaciology, even in the case of isotropic ice. The numerical difficulties arise, first of all, due to the presence of mowing boundaries in the problem, so that the equations are solved on an unknown domain. An additional difficulty is due to the ice incompressibility condition, as it gives rise to unstable solutions when standard numerical techniques are applied. Therefore, instead of attempting to solve the full equations, a more effective approach is to construct an approximate solution by employing the method of asymptotic expansions. The method exploits the small aspect ratio of natural ice masses, ϵ (of a typical magnitude of order 10^{-3}), and, by integration of the balance equations through the ice sheet to eliminate one spatial coordinate, enables significant simplification of the flow equations. Such an approach, known as the Shallow Ice Approximation, or Reduced Model, was pioneered by Fowler and Larson [11], Morland and Johnson [6], and Hutter [12,13], and has found numerous applications ever since. For axially symmetric flows, but of the isotropic ice, the approach was employed by Morland [14] and Cliffe and Morland [15]. Here we apply it to the anisotropic ice flow.

The basis of the method is to perform appropriate scalings: first, to eliminate physical dimensions from the equations by using typical magnitudes of quantities involved, and second, to stretch the horizontal coordinate and velocity so that both, radial and vertical, coordinates and velocity components become order unity. This enables the proper estimation of relative magnitudes of all terms appearing in the flow equations, so that those terms which are less important than other can be eliminated from the analysis. Hence, we adopt characteristic magnitudes: h^*, a typical ice thickness, used as a length unit, and v^*, a typical accumulation rate, used as a velocity unit. These two units determine other scaling parameters: a stress unit $\tau^* = \varrho g h^*$, a strain-rate unit $D^* = v^*/h^*$, a time scale $t^* = h^*/v^* = 1/D^*$, and a viscosity unit $\mu^* = \tau^* h^*/v^*$. By using the adopted scales, we introduce dimensionless variables, indicated by a superposed bar, defined by

$$(\bar{r}, \bar{z}) = (r, z)/h^*,\ (\bar{u}, \bar{w}) = (u, w)/v^*,\ (\bar{\boldsymbol{S}}, \bar{p}) = (\boldsymbol{S}, p)/\tau^*, \quad (\bar{\boldsymbol{L}}, \bar{\boldsymbol{D}}) = (\boldsymbol{L}, \boldsymbol{D})/D^*,\ \bar{t} = t/t^*,\ \bar{\mu}_0 = \mu_0/\mu^*. \tag{30}$$

Further, by means of the parameter ϵ, we stretch the radial coordinate and the radial velocity, leaving the vertical counterparts unchanged, to obtain

$$R = \epsilon\bar{r}, \quad Z = \bar{z}, \quad U = \epsilon\bar{u}, \quad W = \bar{w}. \tag{31}$$

This results in R, Z, U and W all being order unity. We also introduce the normalized free surface and bed profiles, $H(R) = h/h^*$ and $F(R) = f/h^*$ respectively, and their slopes $H'(R) = \Gamma(R)$ and $F'(R) = \beta(R)$, all being order unity as well. The dimensionless stresses defined by (30) are rescaled in an analogous manner, so that

$$\bar{S}_{rr} = \epsilon\Sigma_{rr}, \quad \bar{S}_{\theta\theta} = \epsilon\Sigma_{\theta\theta}, \quad \bar{S}_{zz} = \epsilon\Sigma_{zz}, \quad \bar{S}_{rz} = \epsilon\Sigma_{rz}, \quad \bar{p} = P, \tag{32}$$

where Σ_{ij} are order unity components of a normalized deviatoric stress tensor $\boldsymbol{\Sigma}$.

Application of the above scalings to the mass balance relation (2) yields

$$\frac{\partial U}{\partial R}+\frac{U}{R}+\frac{\partial W}{\partial Z}=0, \tag{33}$$

and the momentum balance equations, (5) and (6), give

$$\epsilon\left(\frac{\partial \Sigma_{rr}}{\partial R}+\frac{\Sigma_{rr}-\Sigma_{\theta\theta}}{R}\right)+\frac{\partial \Sigma_{rz}}{\partial Z}-\frac{\partial P}{\partial R}=0, \tag{34}$$

$$\epsilon^2\left(\frac{\partial \Sigma_{rz}}{\partial R}+\frac{\Sigma_{rz}}{R}\right)+\epsilon\frac{\partial \Sigma_{zz}}{\partial Z}-\frac{\partial P}{\partial Z}=1. \tag{35}$$

In normalized variables, the zero traction conditions (7) and (8) become

$$Z=H(R):\ -\Delta_h^2 P+\epsilon\Sigma_{zz}-2\epsilon^2\Gamma\Sigma_{rz}+\epsilon^3\Gamma^2\Sigma_{rr}=0, \tag{36}$$

$$Z=H(R):(1-\epsilon^2\Gamma^2)\Sigma_{rz}+\epsilon\Gamma(\Sigma_{zz}-\Sigma_{rr})=0, \tag{37}$$

and the free surface kinematic condition (10) takes the form

$$Z=H(R):\quad \Gamma U-W=\Delta_h Q, \tag{38}$$

where $Q=q/v^*$ is a normalized ice accumulation rate. Similarly, the scaled relations for the basal normal and tangential tractions, (11) and (12), become

$$Z=F(R):\Delta_f^2 T_n=-\Delta_f^2 P+\epsilon\Sigma_{zz}-2\epsilon^2\beta\Sigma_{rz}+\epsilon^3\beta^2\Sigma_{rr}, \tag{39}$$

$$Z=F(R):\Delta_f^2 T_s=(1-\epsilon^2\beta^2)\Sigma_{rz}+\epsilon\beta(\Sigma_{zz}-\Sigma_{rr}), \tag{40}$$

where $T_n=t_n/\tau^*$ and $T_s=\epsilon^{-1}t_s/\tau^*$ are scaled basal tractions, both of order unity. The normal and tangential components of the basal velocity, given by (14), are

$$Z=F(R):\ \Delta_f V_n=\beta U-W,\quad \Delta_f V_s=-U-\epsilon^2\beta W, \tag{41}$$

where $V_n=v_n/v^*$ and $V_s=\epsilon v_s/v^*$ denote order unity components of the basal velocity. The kinematic condition at the bed, (15), is defined by

$$Z=F(R):\quad \beta U-W=\Delta_f B, \tag{42}$$

where $B=b/v^*$ is a normalized melt rate. The expressions for Δ_h and Δ_f, see (9) and (13), now have the forms

$$\Delta_h=(1+\epsilon^2\Gamma^2)^{1/2},\quad \Delta_f=(1+\epsilon^2\beta^2)^{1/2}. \tag{43}$$

Further, the sliding law, in physical variables given by (17), in the normalized dimensionless form becomes

$$T_s=\Lambda T_n V_s, \tag{44}$$

where $\Lambda=\epsilon^{-2}v^*\lambda$ is an order unity or greater normalized basal friction coefficient.

Finally, we need the constitutive equation, given by (18), to be expressed in the scaled variables. This requires the strain-rate components (1) to be defined in terms of the stretched variables (31). Accordingly,

$$\bar{D}_{rr}=\frac{\partial U}{\partial R},\quad \bar{D}_{\theta\theta}=\frac{U}{R},\quad \bar{D}_{zz}=\frac{\partial W}{\partial Z},\qquad \bar{D}_{rz}=\frac{1}{2}\left(\epsilon^{-1}\frac{\partial U}{\partial Z}+\epsilon\frac{\partial W}{\partial R}\right), \tag{45}$$

showing that the dominant component, of order ϵ^{-1}, is $\bar{D}_{rz}$. After applying the scalings (30) and (32), the orthotropic constitutive law (18) takes the dimensionless form

$$\boldsymbol{\Sigma}=\epsilon\tilde{\mu}_0\Big\{2\bar{\boldsymbol{D}}+\sum_{s=1}^{3}\tilde{f}(b_s)\big[\boldsymbol{M}^{(s)}\bar{\boldsymbol{D}}+\bar{\boldsymbol{D}}\boldsymbol{M}^{(s)}-\tfrac{2}{3}\,\mathrm{tr}(\boldsymbol{M}^{(s)}\bar{\boldsymbol{D}})\boldsymbol{I}\big]+\tilde{g}(K)\big[\boldsymbol{B}\bar{\boldsymbol{D}}+\bar{\boldsymbol{D}}\boldsymbol{B}-\tfrac{2}{3}\,\mathrm{tr}(\boldsymbol{B}\bar{\boldsymbol{D}})\boldsymbol{I}\big]\Big\}, \tag{46}$$

where $\tilde{\mu}_0$ is a dimensionless normalized viscosity defined by

$$\tilde{\mu}_0=\frac{1}{2}\,a^{-1}(T)\,\psi^{-1}(J). \tag{47}$$

By construction of $a(T)$ and $\psi(J)$, $\tilde{\mu}_0$ is, at near-melting temperatures, an order unity quantity. Since $\tilde{f}(b_s)$ and the components of $\tilde{g}(K)\boldsymbol{B}$ and $\boldsymbol{M}^{(s)}$ $(s=1,2,3)$ are all of order unity, the maximum components of $\bar{\boldsymbol{D}}$ are of order ϵ^{-1}, and on account of the scalings (30) and the definition (23), the value of the small parameter ϵ is determined by

$$\epsilon=\frac{1}{h^*}\left(\frac{\sigma_0 v^*}{\varrho g D_0}\right)^{1/2}. \tag{48}$$

Choosing typical magnitudes of the ice thickness as $h^*=2000$ m and the accumulation rate as $v^*=1\ \mathrm{m\,yr^{-1}}=3.17\times10^{-8}\ \mathrm{m\,s^{-1}}$, with the ice density $\varrho=917\ \mathrm{kg\,m^{-3}}$ and $g=9.81\ \mathrm{m\,s^{-2}}$, the latter relation yields $\epsilon=0.00167\sim1/600$. The invariant J, required to calculate $\tilde{\mu}_0$, when expressed in terms of the normalized stresses Σ_{ij}, becomes

$$J=\vartheta\left[\Sigma_{rz}^2+\tfrac{1}{2}\left(\Sigma_{rr}^2+\Sigma_{\theta\theta}^2+\Sigma_{zz}^2\right)\right],\quad \vartheta=\frac{\varrho g v^*}{\sigma_0 D_0}=0.09. \tag{49}$$

The deviatoric stress components, prescribed by the constitutive law (46), are given by

$$\begin{aligned}
\Sigma_{rr}&=2\tilde{\mu}_0\epsilon\left[(1+2C_1)\bar{D}_{rr}-C_2\bar{D}_{\theta\theta}-C_3\bar{D}_{zz}+C_4\bar{D}_{rz}\right],\\
\Sigma_{\theta\theta}&=2\tilde{\mu}_0\epsilon\left[-C_1\bar{D}_{rr}+(1+2C_2)\bar{D}_{\theta\theta}-C_3\bar{D}_{zz}-2C_4\bar{D}_{rz}\right],\\
\Sigma_{zz}&=2\tilde{\mu}_0\epsilon\left[-C_1\bar{D}_{rr}-C_2\bar{D}_{\theta\theta}+(1+2C_3)\bar{D}_{zz}+C_4\bar{D}_{rz}\right],\\
\Sigma_{rz}&=2\tilde{\mu}_0\epsilon\left[C_4(\bar{D}_{rr}+\bar{D}_{zz})+(1+C_5)\bar{D}_{rz}\right],
\end{aligned} \tag{50}$$

where the coefficients C_i $(i=1,\ldots,5)$ are defined by

$$\begin{aligned}
C_1&=\tfrac{1}{3}\left[\tilde{f}(b_1)M_{rr}^{(1)}+\tilde{f}(b_3)M_{rr}^{(3)}+\tilde{g}(K)B_{rr}\right],\\
C_2&=\tfrac{1}{3}\left[\tilde{f}(b_2)+\tilde{g}(K)B_{\theta\theta}\right],\\
C_3&=\tfrac{1}{3}\left[\tilde{f}(b_1)M_{zz}^{(1)}+\tilde{f}(b_3)M_{zz}^{(3)}+\tilde{g}(K)B_{zz}\right],\\
C_4&=\tfrac{1}{3}\left[\tilde{f}(b_1)M_{rz}^{(1)}+\tilde{f}(b_3)M_{rz}^{(3)}+\tilde{g}(K)B_{rz}\right],\\
C_5&=\tfrac{1}{2}\left[\tilde{f}(b_1)+\tilde{f}(b_3)+\tilde{g}(K)(B_{rr}+B_{zz})\right].
\end{aligned} \tag{51}$$

The above coefficients describe the strength of anisotropy of the fabric. In undeformed state, when $\boldsymbol{B}=\boldsymbol{I}$, all these coefficients become zero, which is ensured by the construction of the functions $\tilde{f}$ and $\tilde{g}$ [5,7]. Then, the relations (50) yield

$\Sigma_{ij} = 2\tilde{\mu}_0 \epsilon \bar{D}_{ij}$, which is the viscous flow law for an isotropic fluid.

In order to follow the evolution of the fabric, described by (27), we also need the components of $\boldsymbol{F}$ and $\boldsymbol{L}$ to be expressed in the stretched coordinates. These are

$$F_{rr} = \frac{\partial R}{\partial R^*}, \quad F_{\theta\theta} = \frac{R}{R^*}, \quad F_{zz} = \frac{\partial Z}{\partial Z^*}, \\ F_{rz} = \epsilon^{-1} \frac{\partial R}{\partial Z^*}, \quad F_{zr} = \epsilon \frac{\partial Z}{\partial R^*}, \tag{52}$$

where $R^* = \epsilon r^*/h^*$ and $Z^* = z^*/h^*$ are the stretched reference coordinates, and

$$\bar{L}_{rr} = \frac{\partial U}{\partial R}, \quad \bar{L}_{\theta\theta} = \frac{U}{R}, \quad \bar{L}_{zz} = \frac{\partial W}{\partial Z}, \\ \bar{L}_{rz} = \epsilon^{-1} \frac{\partial U}{\partial Z}, \quad \bar{L}_{zr} = \epsilon \frac{\partial W}{\partial R}. \tag{53}$$

5. Leading-order solutions

We now construct an approximate solution of the equations that are derived in the preceding section in the form of expansions in the small parameter $\epsilon \ll 1$. To this aim, we first neglect in the full equations all terms which are of order ϵ or smaller compared to unity, and then solve the simplified equations to obtain the leading-order solution of the flow problem. The approximate solution is constructed under the standard *Reduced Model* assumption that the bed slopes $f'(r)$ are of order ϵ or less, that is, the normalized slopes $\beta = F'(R)$ are of order unity or less [6,13]. The situations in which the bed slopes are of larger magnitudes have been treated, for isotropic ice, by Morland [16] and Schoof [17].

Hence, we simplify the relevant equations from Section 4 by omitting all terms with the factors ϵ, ϵ^2 and ϵ^3, considering them to be negligibly small. The mass conservation balance equation (33), as it does not involve ϵ, is solved in its full form. The horizontal and vertical equilibrium equations, (34) and (35), become

$$\frac{\partial P}{\partial R} = \frac{\partial \Sigma_{rz}}{\partial Z}, \quad \frac{\partial P}{\partial Z} = -1. \tag{54}$$

The expressions (43), due to the assumption that the normalized free surface and bed slopes, Γ and β respectively, do not exceed unity, yield

$$\Delta_h = 1, \quad \Delta_f = 1. \tag{55}$$

Therefore, the free surface zero traction conditions, defined by (36) and (37), become, to leading order,

$$Z = H(R): \quad P = 0, \quad \Sigma_{rz} = 0, \tag{56}$$

and the free surface kinematic condition is

$$Z = H(R): \quad \Gamma U - W = Q. \tag{57}$$

At the bed $Z = F(R)$, the normal and tangential traction components, (39) and (40), are expressed, to leading order, by

$$Z = F(R): \quad T_n = -P, \quad T_s = \Sigma_{rz}, \tag{58}$$

the velocity components, (41), are now given by

$$Z = F(R): \quad V_n = \beta U - W, \quad V_s = -U, \tag{59}$$

and the basal kinematic condition, (42), is

$$Z = F(R): \quad \beta U - W = B. \tag{60}$$

With the basal tractions and velocities defined by (58) and (59), the leading-order form of the sliding law (44) is expressed by

$$Z = F(R): \quad \Sigma_{rz} = \Lambda P U. \tag{61}$$

The deviatoric stress components are prescribed by expressions (50) and (51). The coefficients C_i $(i = 1, \ldots, 5)$ define changes in the viscosities relative to unity as ice evolves from initially isotropic to fully anisotropic fabric. Experimental evidence shows that the ice viscosities do not vary by more than a factor of 10. On the other hand, as indicated by relations (45), the shear strain-rates $\bar{D}_{rz}$ are by the factor of $\epsilon^{-1} \sim 600 \gg 10$ greater than each of the axial strain-rates. This implies that in strongly anisotropic fabrics all the components Σ_{ij} are of the same order, governed by the magnitude of $\bar{D}_{rz}$. Accordingly, the leading-order relations for the deviatoric stresses are given by

$$\Sigma_{rr} = \Sigma_{zz} = \\ -\frac{1}{2}\Sigma_{\theta\theta} = \tilde{\mu}_0 C_{rr} \frac{\partial U}{\partial Z}, \quad \Sigma_{rz} = \tilde{\mu}_0 C_{rz} \frac{\partial U}{\partial Z}, \tag{62}$$

where

$$C_{rr} = C_4, \\ C_{rz} = 1 + \frac{1}{2}\left[\tilde{f}(b_1) + \tilde{f}(b_3) + \tilde{g}(K)(B_{rr} + B_{zz})\right]. \tag{63}$$

For the isotropic ice, $C_{rr} = 0$ and $C_{rz} = 1$. With increasing strength of anisotropy, C_{rr} grows, while C_{rz} decreases (but remains positive). The normalized stress invariant J, given by (49), becomes, to leading order,

$$J = \vartheta \Sigma_{rz}^2 (1 + 3\alpha^2), \quad \alpha = C_{rr}/C_{rz}. \tag{64}$$

In order to solve the above leading-order equations, we, essentially, follow the method applied in [14,16]. The new features in this analysis are: (1) the inclusion of the ice anisotropy in the flow problem, (2) no stream function is used to construct the solution, and (3) a different method is applied to solve the ensuing differential equation for the free surface elevation function $H(R)$. Hence, we start from integration of equations (54) with the boundary conditions (56), which yields the pressure and shear stress fields

$$P(R, Z) = H(R) - Z, \quad \Sigma_{rz}(R, Z) = -\Gamma(R)[H(R) - Z]. \tag{65}$$

These two relations define the pressure P_b and shear stress Σ_{rzb} at the base $Z = F(R)$ as

$$P_b(R) = \Delta(R), \quad \Sigma_{rzb}(R) = -\Gamma(R)\Delta(R), \\ \Delta(R) = H(R) - F(R), \tag{66}$$

where $\Delta(R)$ is the ice thickness. With the latter stress components, the sliding law (61) determines the leading-order horizontal velocity at the base, U_b, as

$$U_b(R) = -\frac{\Gamma(R)}{\Lambda(R)}, \tag{67}$$

where it is assumed that the friction coefficient Λ depends only on the position R, that is, does not depend on stress and temperature. The kinematic condition at the bed, (60), expresses then the basal vertical velocity W_b by

$$W_b(R) = \beta(R)U_b(R) - B(R), \tag{68}$$

where the basal melt rate is assumed to depend only on R. The basal velocity components (67) and (68) are used as boundary conditions in integration of the flow equations over the depth Z in order to determine the velocity field inside the ice sheet. Accordingly, we eliminate Σ_{rz} from $(65)_2$ by using the last of the constitutive relations (62), and then, by integrating the resulting equation for U, we obtain

$$U(R,Z) = U_b(R) + G_1(R,Z), \tag{69}$$

where the function G_1 is defined by

$$G_1(R,Z) = -\Gamma(R)\int_F^Z \frac{H(R)-Z'}{\tilde{\mu}_0(R,Z')C_{rz}(R,Z')}\,\mathrm{d}Z'. \tag{70}$$

The prime denotes a running integration variable. With the horizontal velocity component U given by (69), the vertical component W is calculated from the incompressibility equation (33). Thus,

$$\begin{aligned} &W(R,Z) = \\ &W_b(R) - \frac{1}{R}\,U_b(R)[Z-F(R)] - \frac{\mathrm{d}U_b}{\mathrm{d}R}\,[Z-F(R)] \\ &-\frac{1}{R}\,G_2(R,Z) - \frac{\partial G_2}{\partial R}(R,Z), \end{aligned} \tag{71}$$

where

$$G_2(R,Z) = -\Gamma(R)\int_F^Z \frac{(Z-Z')(H-Z')}{\tilde{\mu}_0(R,Z')C_{rz}(R,Z')}\,\mathrm{d}Z'. \tag{72}$$

The above leading-order relations express the stress and velocity components in terms of the free surface elevation function $H(R)$, which is yet unknown, and the given bed elevation function $F(R)$. In order to find $H(R)$, we make use of the kinematic conditions (57) and (60), prescribed at the surface and the bed, respectively. Hence, we first difference both equations, and then substitute the expressions for U and W, (69) and (71), into the resulting relation. This yields the differential equation

$$\frac{\mathrm{d}}{\mathrm{d}R}\left\{RU_b(R)\,\Delta(R) - R\Gamma(R)I(R)\right\} = RQ^*[R,H(R)], \tag{73}$$

where $Q^* = Q - B$, and $I(R)$ is defined by

$$I(R) = \int_{F(R)}^{H(R)} \frac{(H-Z')^2}{\tilde{\mu}_0(R,Z')\,C_{rz}(R,Z')}\,\mathrm{d}Z'. \tag{74}$$

Integration of (73) from the divide $R = 0$ to the margin $R = R_M$, due to $I(R_M) = 0$, gives the relation

$$\int_0^{R_M} RQ^*[R,H(R)]\,\mathrm{d}R = 0, \tag{75}$$

stating that there is no net flux of mass into the sheet. In other words, the global mass of ice remains constant, which is consistent with the steady flow assumption.

Equation (73) is second-order for the function $H(R)$, since $\Delta(R) = H(R) - F(R)$ and $\Gamma(R) = H'(R)$. We solve (73) by transforming it into an equivalent set of two first-order equations. To this aim, denote the expression in curly braces in (73) by

$$K(R) = -R\Gamma(R)\left\{\Lambda^{-1}(R)\,\Delta(R) + I(R)\right\}, \tag{76}$$

where we have substituted (67) for U_b. Then, (73) becomes a first-order equation

$$\frac{\mathrm{d}K}{\mathrm{d}R} = RQ^*[R,H(R)]. \tag{77}$$

This equation is solved over R ranging from zero to the margin at R_M. Since at $R = R_M$ $\Delta = 0$, hence $I(R) = 0$ and $K = 0$, the boundary conditions for (77) are expressed by

$$K(0) = 0, \quad K(R_M) = 0. \tag{78}$$

In terms of K, (76) expresses $\Gamma(R) = H'(R)$ as

$$\frac{\mathrm{d}H}{\mathrm{d}R} = -\frac{K(R)}{R\left\{\Lambda^{-1}(R)\,\Delta(R) + I(R)\right\}}, \tag{79}$$

which is the other first-order equation, to be solved along with (77). The boundary conditions for (79) are defined by

$$H(0) = H_D, \quad H(R_M) = F(R_M), \tag{80}$$

where H_D is the free surface elevation at the ice sheet centre (which is called the ice divide), and R_M is the place where $H = F$, that is, $\Delta = 0$; both H_D and R_M are unknown quantities that need to be calculated as part of the solution.

We note in passing that the mechanism of the anisotropic fabric evolution is represented in our leading-order solutions by the two functions C_{rz} and C_{rr} which enter the denominators of the integrands in (70), (72) and (74) (C_{rr} is involved implicitly through the invariant J, see (47) and (64)).

6. Numerical calculations and illustrations

The two first-order differential equations (77) and (79) for the free surface profile $H(R)$ form, in view of the conditions (78) and (80), a two-point boundary-value problem. The fact that the position of one of the endpoints, the margin R_M, is unknown adds substantially to the numerical complexity of the problem. A shooting method has been applied to solve the equations. First, for given distributions of the fabric functions C_{rz} and C_{rr}, trial values of H_D and R_M are assumed, and then, starting from the endpoints $R = 0$ and $R = R_M$ and moving inwards, numerical integration is carried out by using a Runge-Kutta-Fehlberg scheme with an adaptive step size. The routine is repeated until the elevation H and the value of the function K are matched at a chosen interior fitting point. The validity and accuracy of the solution obtained is verified by employing the integral property (75). Having found H, the flow field variables (the velocities and their gradients) are evaluated and the distributions of the functions C_{rz} and C_{rr} are updated, before starting calculations to find the next approximation for H. Such iterations between the fabric and the flow

fields are repeated until a convergent solution is obtained; the first iteration is started from the isotropic fabric, for which $C_{rz} = 1$ and $C_{rr} = 0$. Simultaneously, in each iteration, a set of five hyperbolic partial differential equations defined by (27) is solved to follow the evolution of the fabric along ice particle paths (streamlines). The paths start at the free surface in the accumulation zone ($Q > 0$), where $\boldsymbol{F} = \boldsymbol{I}$, pass through the interior of the ice sheet, and end either at the free surface in the ablation zone ($Q < 0$), or at the bed if basal melting occurs ($B > 0$). In calculations, 500 basic integration points along R were used to solve (77) and (79) for $K(R)$ and $H(R)$, 100 points along the vertical were applied to perform all depth integrations, and up to about 5000 basic intervals were needed to calculate deformation gradients along the longest characteristics (streamlines).

The results presented below have been obtained for the flat, horizontal bed, $F = 0$. The adopted characteristic magnitudes are $h^* = 2000$ m and $v^* = 1$ m yr^{-1}, implying $\epsilon = 0.00167 \sim 1/600$, so that the length unit in the radial direction is 1200 km, and the horizontal velocity unit is 600 m yr^{-1}. The basal friction coefficient is $\Lambda = 10$. The ice accumulation distribution function Q has been adopted in the form proposed by Morland [14]

$$Q = Q_\infty - (Q_\infty - Q_0)\exp(-H/H^*), \qquad (81)$$

where Q_∞ and Q_0 define the accumulation rates at $H \to \infty$ and $H = 0$ respectively, and H^* is a decay height. In the simulations the values $Q_\infty = 0.5$, $Q_0 = -1$, and $H^* = 0.25$ have been used. No basal melt has been assumed, so $B = 0$ and $Q^* = Q$. The adopted temperature distribution function, also from [14], is expressed by

$$T_1 = -\tfrac{4}{5}H + \tfrac{1}{2}(H - Z)\left\{1 - \tfrac{1}{4}\Delta\left[\Delta - \tfrac{1}{2}(H - Z)\right]\right\}. \qquad (82)$$

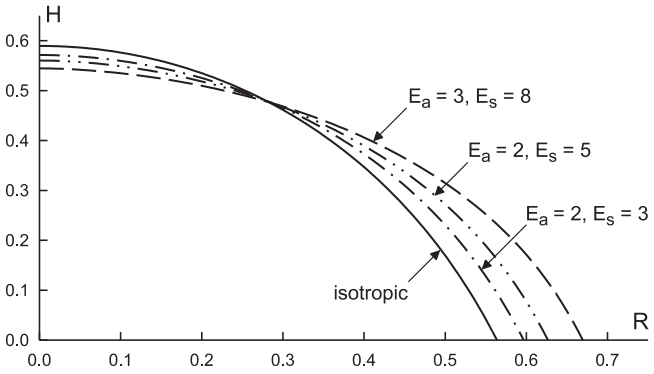

Fig. 2. Free surface profiles $H(R)$ for isotropic and anisotropic ice with different combinations of enhancement factors E_a and E_s

As first, in Fig. 2 we illustrate the effect of the ice anisotropy on the free surface profile $H(R)$. Shown are the results obtained for different combinations of enhancement factors, E_a and E_s, defining the limit strength of anisotropy in compression and shear (for isotropic ice both E_a and E_s are unity). The combination of $E_a = 3$ and $E_s = 8$ has been measured in laboratory and describes the viscous properties of so-called warm ice [18,2], that is the ice at near melting temperatures and high strain-rates, at which some recrystallization processes that enhance the ice deformation are active. The results presented indicate that the influence of the ice anisotropy is more pronounced on the ice sheet extent R_M, than on the ice thickness H_D at the divide $R = 0$. For the most anisotropic ice illustrated in the figure (dashed line), the sheet span increases by about 19% compared to the isotropic ice (solid line), while the divide thickness decreases by about 8%. In physical units, this is equivalent to the span increase by 127 km, and the divide thickness decrease by 90 m.

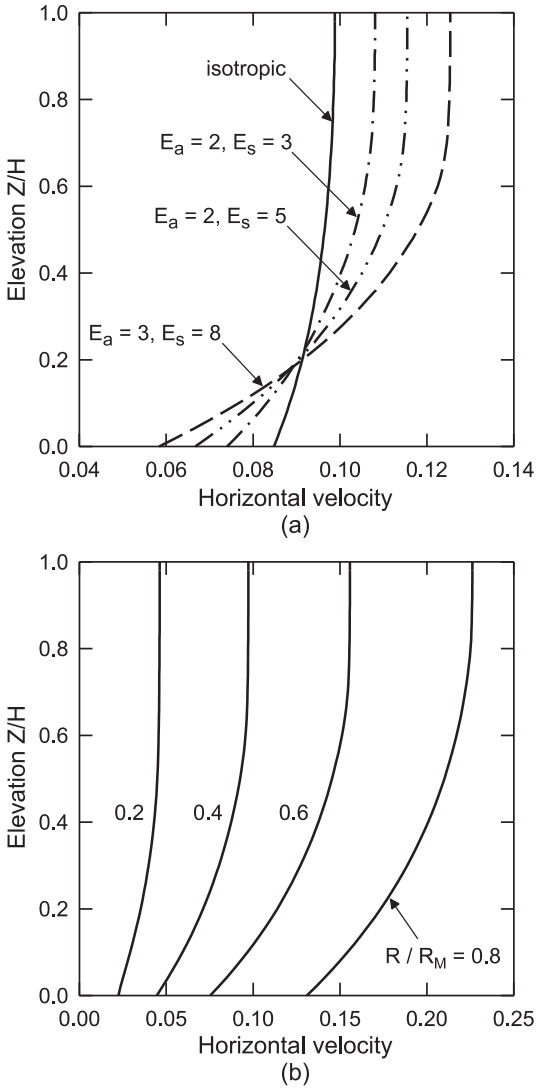

Fig. 3. Horizontal velocity depth profiles: (a) at $R = R_M/2$ for isotropic and anisotropic ice with different combinations of enhancement factors; (b) at different locations R/R_M for anisotropic ice defined by the factors $E_a = 3$ and $E_s = 8$

In Fig. 3 we show depth profiles of the scaled horizontal velocity U, plotted against the normalized elevation Z/H. In Fig. 3a the velocity profiles at $R = R_M/2$, for the same ice sheet geometry and the types of ice as those illustrated in Fig. 2, are compared. We observe that the anisotropy of ice significantly affects the velocity field across the glacier. An interesting feature is the decrease of the basal horizontal velocity U_b with increasing E_s, that is, with increasing ease of shear, so

that the fastest flowing ice near the bed is the isotropic (i.e., the 'stiffest') ice. On the other hand, the fastest flowing ice at the free surface is, as could be expected, the most anisotropic one. Figure 3b displays the distributions of the velocity U at different locations R/R_M in the flow of ice defined by the enhancement factors $E_a = 3$ and $E_s = 8$. We note that the velocities vary considerably down the ice sheet, growing steadily with increasing distance from the divide. The latter is a consequence of the increasing area of the accumulation zone between the divide and a given location R, requiring increasing horizontal velocities to transport the ice from the central region of the glacier towards its margin.

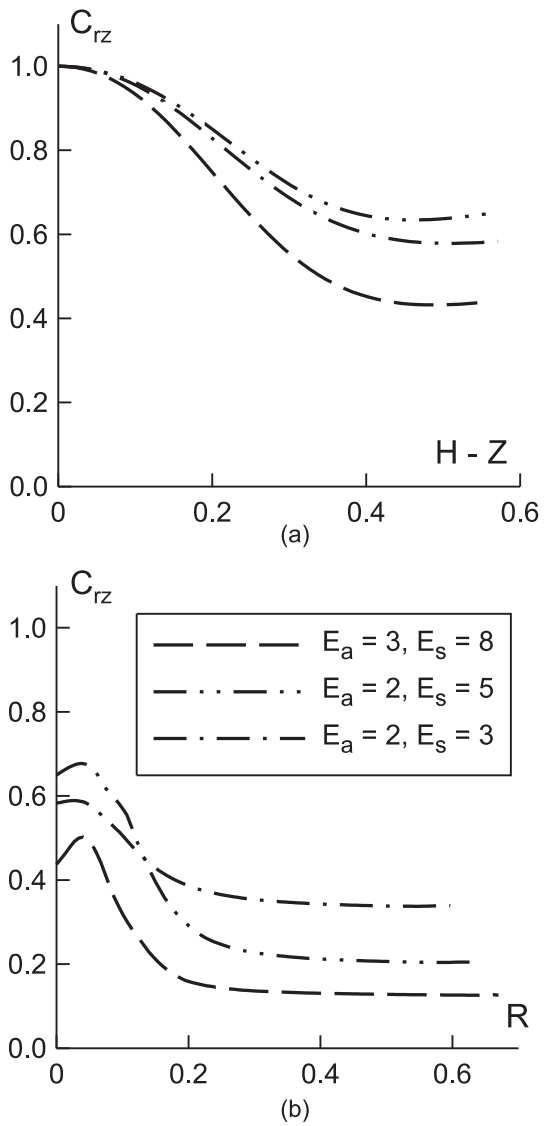

Fig. 4. Distributions of the viscosity factor C_{rz}: (a) along the symmetry axis Z and (b) along the bed $F = 0$, for anisotropic ice with different enhancement factors E_a and E_s

Figure 4 illustrates the variation of the function C_{rz} down the ice divide (the symmetry axis Z) and along the ice base $F = 0$, for the same anisotropic ice parameters as those used in the previous plots (for the isotropic ice this function is identically unity). The function C_{rz} serves as a factor multiplying the isotropic ice viscosity $\tilde{\mu}_0$, as can be seen in the relevant relations derived in Section 5. Hence, the magnitude of C_{rz} indicates how the ice shear viscosity changes compared to $\tilde{\mu}_0$ as the anisotropic fabric evolves in the material. We see in the plots (a) that the viscosity decreases in a monotonic manner as the ice, undergoing uni-axial compression, descends down the divide. Reaching the bed, the ice deforms mainly by shearing, with its rate increasing with the distance from the divide $R = 0$. The growing shear deformation leads to the reduction of the shear resistance of the medium, reflected by the progressive decrease in the shear viscosity, until a limit value has been attained. This mechanism is demonstrated well by the plots (b), showing that the ice at the most part of the glacier base has a nearly constant viscosity, equal to the limit shear viscosity (for which the viscosity factor is given by $C_{rz} = 1/E_s$, equal to 0.125 for the most anisotropic ice, illustrated by the dashed line).

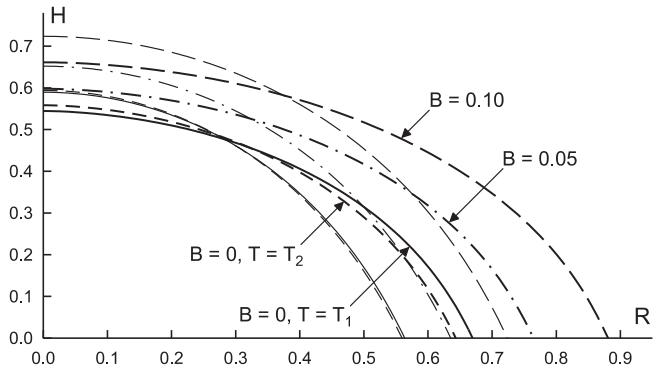

Fig. 5. Free surface profiles $H(R)$ for flows with different basal melt rates B and temperature distributions T, for anisotropic ice defined by the enhancement factors $E_a = 3$ and $E_s = 8$. Corresponding isotropic ice profiles are plotted in thin lines

Finally, in Fig. 5 we show the effects of basal melt rate and the temperature distribution on the ice sheet geometry. Presented are the free surface profiles for the flows of the most anisotropic ice ($E_a = 3$ and $E_s = 8$) for three different melt rates, $B = 0$ (no basal melt), $B = 0.05$ and $B = 0.10$, all for the temperature distribution T_1 given by (82). Additionally, we also show the surface profile $H(R)$ for no basal melting, but with a different temperature distribution, denoted by T_2. The latter is the distribution in which the ice is assumed to have, at a given R, a constant temperature that is an average of the corresponding surface and base temperatures prescribed by (82). Hence, T_2 defines the surface temperature which is higher, and the base temperature which is lower, than the respective temperatures given by T_1. In the figure, the profiles for the anisotropic ice (plotted in heavy lines) are compared with the corresponding results for the isotropic ice (thin lines in matching styles). We note that the presence of basal melting significantly increases the volume of ice in steady flow, increasing both the lateral span R_M and the divide thickness H_D by approximately the same rates when compared to the no basal melt flow. The comparison of the free surface profiles for the anisotropic and isotropic ice indicates that the anisotropy

effects, reflected by flattening of the sheet, are similar in the three cases of B investigated. Therefore, it appears that the basal melting does not modify considerably the overall behaviour of the anisotropic ice sheet. The plots for $B = 0$ and two different temperature distributions, T_1 and T_2, demonstrate that the influence of temperature is moderate, leading to a relative decrease in the radial span R_M by about 4% for the distribution T_2, that is, when the ice at the glacier base is colder, and hence more viscous, than it is in the case of the temperature field T_1.

7. Conclusions

We have analysed a steady, axially symmetric polar ice sheet flow problem in which, for given bed topography, temperature field, basal melt conditions and ice accumulation/ablation rates, an a priori unknown geometry of the free surface of the sheet is sought. The major feature in this study, compared to the conventional isotropic ice models, is the incorporation in the analysis of the mechanism of evolving anisotropy of ice. The flow problem has been simplified by applying a method of asymptotic expansions, and the resulting two-point boundary-value problem for leading-order differential equations has been solved, on an initially unknown domain, by a numerical method.

The results of simulations, performed for experimentally measured rheological parameters pertaining to the ice which is known in glaciology as 'warm ice', show that the anisotropy of the medium plays a significant role in the flow of glaciers. The free surface profiles for the anisotropic ice are distinctly flatter than those for the isotropic ice. For the ice accumulation and temperature distributions adopted in the calculations, the predicted lateral extent of the anisotropic ice sheet is about one-fifth greater than that in the case of the isotropic ice, and the maximum ice thickness is about one-tenth smaller, respectively. The velocity profiles across the depth of the ice are also affected by the evolution of the ice fabric: the basal horizontal velocities for the anisotropic ice are significantly smaller, and the free surface velocities are significantly greater, than the corresponding quantities for the isotropic ice. The occurrence of ice melting at the base has proved to be little important in terms of the normalized velocity distributions in the ice sheet, though it has a considerable effect on the overall volume of the glacier in steady flow.

We have applied here a constitutive law which accounts for the mechanism of ice crystal lattice rotation. Future theoretical and numerical developments should also attempt to include other phenomena that can influence the overall behaviour of polar ice sheets. First of all, the microprocesses of so-called migration recrystallization and crystal polygonization should be incorporated in the ice flow analysis. However, satisfactory constitutive equations for the description of such processes have not been formulated yet, and without these equations no significant progress in the area of large-scale polar ice sheet modelling is possible.

Acknowledgements. Significant part of the theoretical results presented in this paper was obtained during a project *Evolving Anisotropy in Ice Sheet Flows* supported by EPSRC (United Kingdom).

References

[1] T. Thorsteinsson, J. Kipfstuhl, and H. Miller, "Textures and fabrics in the GRIP ice core", *J. Geophys. Res.* 102(C12), 26583–26599 (1997).

[2] W. F. Budd and T. H. Jacka, "A review of ice rheology for ice sheet modelling", *Cold Reg. Sci. Technol.* 16(2), 107–144 (1989).

[3] A. Mangeney, F. Califano, and O. Castelnau, "Isothermal flow of an anisotropic ice sheet in the vicinity of an ice divide", *J. Geophys. Res.* 101(B12), 28189–28204 (1996).

[4] A. Mangeney, F. Califano, and K. Hutter, "A numerical study of anisotropic, low Reynolds number, free surface flow for ice sheet modeling", *J. Geophys. Res.* 102(B10), 22749–22764 (1997).

[5] R. Staroszczyk and L. W. Morland, "Strengthening and weakening of induced anisotropy in polar ice", *Proc. R. Soc. Lond. Ser. A* 457(2014), 2419–2440 (2001).

[6] L. W Morland and I. R. Johnson, "Steady motion of ice sheets", *J. Glaciol.* 25(92), 229–246 (1980).

[7] R. Staroszczyk, *Constitutive Modelling of Creep Induced Anisotropy of Ice*, IBW PAN Publishing House, Gdańsk, 2004.

[8] R. Staroszczyk and L. W. Morland, "Orthotropic viscous response of polar ice", *J. Eng. Math.* 37(1-3), 191–209 (2000).

[9] L. W. Morland and R. Staroszczyk, "Stress and strain-rate formulations for fabric evolution in polar ice", *Continuum Mech. Thermodyn.* 15(1), 55–71 (2003).

[10] G. D. Smith and L. W. Morland, "Viscous relations for the steady creep of polycrystalline ice", *Cold Reg. Sci. Technol.* 5(2), 141–150 (1981).

[11] A. C. Fowler and D. A. Larson, "On the flow of polythermal glaciers. I. Model and preliminary analysis", *Proc. R. Soc. Lond. Ser. A* 363(1713), 217–242 (1978).

[12] K. Hutter, "The effect of longitudinal strain on the shear stress of an ice sheet: in defence of using stretched coordinates", *J. Glaciol.* 27(95), 39–56 (1981).

[13] K. Hutter, *Theoretical Glaciology. Material Science of Ice and the Mechanics of Glaciers and Ice Sheets*, Reidel, Dordrecht, 1983.

[14] L. W. Morland, "Radially symmetric ice sheet flow", *Phil. Trans. R. Soc. Lond. Ser. A* 355, 1873–1904 (1997).

[15] K. A. Cliffe and L. W. Morland, "Full and reduced model solutions of steady axi-symmetric ice sheet flow over bed topography with moderate slopes", *Continuum Mech. Thermodyn.* 14(2), 149–164 (2002).

[16] L. W. Morland, "Steady plane isothermal linearly viscous flow of ice sheets on beds with moderate-slope topography", *Proc. R. Soc. Lond. Ser. A* 456(1999), 1711–1739 (2000).

[17] C. Schoof, "The effect of basal topography on ice sheet dynamics", *Continuum Mech. Thermodyn.* 15(3), 295–307 (2003).

[18] T. H. Jacka, "The time and strain required for development of minimum strain rates in ice", *Cold Reg. Sci. Technol.* 8(3), 261–268 (1984).